

Complex Three-Dimensional Magnetic Ordering in Segmented Nanowire Arrays

Alexander J. Grutter,^{*,†} Kathryn L. Krycka,[†] Elena V. Tartakovskaya,^{‡,§} Julie A. Borchers,[†] K. Sai Madhukar Reddy,^{||} Eduardo Ortega,[⊥] Arturo Ponce,[⊥] and Bethanie J. H. Stadler^{||}

[†]NIST Center for Neutron Research, National Institute of Standards and Technology, Gaithersburg, Maryland 20899, United States

[‡]Institute of Magnetism, NASU of Ukraine, 03142 Kiev, Ukraine

[§]Kiev National University, Institute of High Technologies, 03022 Kiev, Ukraine

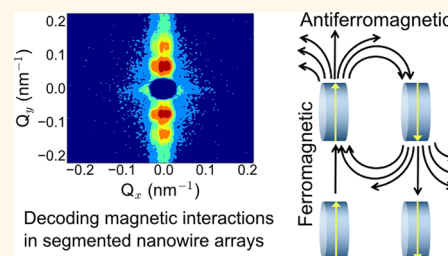
^{||}Department of Electrical and Computer Engineering, University of Minnesota, Minneapolis, Minnesota 55455, United States

[⊥]Department of Physics and Astronomy, University of Texas at San Antonio, San Antonio, Texas 78249, United States

Supporting Information

ABSTRACT: A comprehensive three-dimensional picture of magnetic ordering in high-density arrays of segmented FeGa/Cu nanowires is experimentally realized through the application of polarized small-angle neutron scattering. The competing energetics of dipolar interactions, shape anisotropy, and Zeeman energy in concert stabilize a highly tunable spin structure that depends heavily on the applied field and sample geometry. Consequently, we observe ferromagnetic and antiferromagnetic interactions both among wires and between segments within individual wires. The resulting magnetic structure for our nanowire sample in a low field is a fan with magnetization perpendicular to the wire axis that aligns nearly antiparallel from one segment to the next along the wire axis. Additionally, while the low-field interwire coupling is ferromagnetic, application of a field tips the moments toward the nanowire axis, resulting in highly frustrated antiferromagnetic stripe patterns in the hexagonal nanowire lattice. Theoretical calculations confirm these observations, providing insight into the competing interactions and resulting stability windows for a variety of ordered magnetic structures. These results provide a roadmap for designing high-density magnetic nanowire arrays for spintronic device applications.

KEYWORDS: magnetism, segmented nanowires, nanowire array, galfenol, polarization analyzed small-angle neutron scattering, dipole interactions, magnetic coupling



High-density arrays of ferromagnetic nanowires are critical to making next-generation 3D spintronic technologies a reality. Among these highly desirable device architectures is spin transfer torque-based racetrack memory, which relies on the 3D scaling of arrays to increase information density.^{1–4} In particular, segmented or thickness-modulated nanowires have emerged very recently as exciting routes toward magnetic memory.^{5,6} Beyond memory, arrays of magnetostrictive nanowires are ideal as catalysts or functional elements in nanoscale actuators and nanoelectromechanical systems (NEMS) for biomimetic applications.^{7–14} Galfenol alloys (Fe_{1-x}Ga_x, $x = 0.1–0.4$) have attracted a great deal of interest for this purpose due to their high ductility, strength, and giant magnetostrictive properties.^{15–17} Thus, engineering high-density arrays of ferromagnetic nanowires is among the most promising routes toward integrating nanostructures into magnetic device architectures.^{7,10,18,19}

A key step in realizing these devices is the demonstration of large-area, highly uniform nanowire arrays, a milestone that we have recently achieved through electrochemical deposition of segmented FeGa wires.^{20–22} To attain the anticipated densities,

nanowires within the array must be in close proximity to each other. Most theoretical treatments of 3D domain structures are based on noninteracting wires, although some approach arrays as continuums that vary from individual nanowires to thin films as a function of porosity.²³ Neither assumption is fully appropriate for close-packed segmented nanowire arrays in which the combination of intersegment and interwire interactions results in the formation of long-range magnetic correlations. Theoretical treatments by Agramunt-Puig *et al.* noted that interwire and intersegment interactions have important implications for collective behavior such as magnetic reversal,²⁴ but did not address the formation of long-range magnetic structures in intermediate fields. Thus, the nature of the magnetic configurations stabilized by competing interactions in closely packed nanowire arrays is largely unexplored. Intersegment interactions have been studied in individual

Received: May 18, 2017

Accepted: July 12, 2017

Published: July 12, 2017



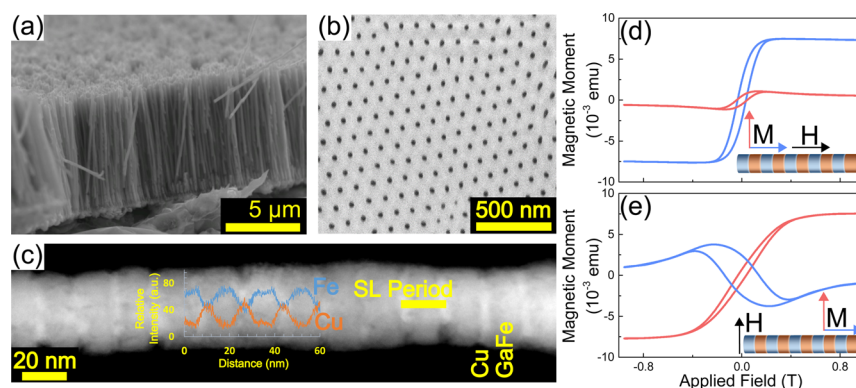


Figure 1. (a) Scanning electron micrograph (SEM) of a high-density nanowire array with AAO removed. (b) SEM of the top of an AAO template. (c) HAADF image of a FeGa/Cu nanowire with EDS line scan analysis for Fe and Cu superimposed on the measured region. (d) Uncorrected magnetization parallel (blue) and perpendicular (red) to the nanowire axis vs applied field hysteresis loops measured using vibrating sample magnetometry with the field applied along the nanowire axis or (e) perpendicular to the nanowire axis ($1 \text{ memu} = 1 \text{ nA}\cdot\text{m}^2$).

nanowires, such as recent reports that show that competition between shape anisotropy and intersegment magnetic interactions in FeGa/Cu nanowires can be tuned by varying segment aspect ratios.^{25–27} However, these individual nanowires were examined by scanning probe techniques, which cannot be utilized for *in situ* magnetic characterization of interactions throughout 3D nanowire arrays. Only a 3D examination technique such as polarization-analyzed small-angle neutron scattering (PASANS) can validate 3D ordering from all competing energetics, such as segment shape anisotropy, intersegment dipole interactions, and interwire dipole interactions. Recently, SANS has been successfully used to probe arrays of continuous magnetic nanowires.^{28–30} Napolskii *et al.*²⁸ noted that SANS could compare magnetic and structural periodicity, while Günther *et al.*²⁹ and Maurer *et al.*³⁰ observed indications of nonuniform magnetization or core/shell spin configurations within continuous nanowires.

Here, we present an exceptional 3D picture of magnetic structures in high-density segmented FeGa/Cu magnetic nanowires in an array, obtained using PASANS. We further present a theoretical treatment that will form a basis for engineering more complex functional magnetic structures. We show that the interactions and anisotropies of segmented nanowires in arrays are controlled by the aspect ratios of the FeGa and Cu segments. Depending on these ratios, the magnetic easy axis of the array can be rotated relative to the nanowire axis, as found by Piroux,²³ and the segments will correspondingly interact to varying degrees. The interwire interactions greatly impact high-density applications, where each nanowire is expected to contain independent information. The magnetic morphologies resulting from these complex interactions are difficult to measure with standard characterization tools; yet the sensitivity of neutrons to magnetic moments provides an avenue for such interactions to be observed, as will be demonstrated here.

RESULTS

High-density arrays of segmented FeGa/Cu nanowires (Figure 1a) were prepared by electrodeposition into porous anodic aluminum oxide (AAO).^{20,21} As shown in Figure 1b, the pores are ordered over $\sim 1 \mu\text{m}$ in a 2-D hexagonal lattice but do not retain longer range order across the entire sample. Pore and nanowire diameters were engineered to be 35 nm,²⁰ while interwire spacing was maintained at 100 nm. On the basis of

past results, the standard deviation in segment length is expected to be less than 3%.²⁰ By adjusting the deposition potential, the relative deposition rates of the constituent materials can be precisely tuned, resulting in co-deposition of nanowires with less than 1% percent contamination from adjacent segments.³¹ This control is accomplished through low concentrations of the more noble metal in the synthesis electrolyte. Here, FeGa segments with 80:20 = Fe:Ga were spaced by pure Cu segments.²¹ The intersegment periodicity was determined through scanning transmission electron microscopy (STEM) measurements, where the Z contrast was observed in Figure 1c by high-angle annular dark field (HAADF) imaging and by energy dispersive spectroscopy (EDS), where the Cu–K signal peaks alternated with the Fe–K and Ga–K peaks on the line scan performed over the nanowire (inset). STEM confirms that the segments are relatively uniform and the interfaces are locally well-defined. Statistical analysis of approximately 100-layer images reveals that the FeGa/Cu segment thicknesses were $(11.6/5.0)_{350} \text{ nm}$ with a superlattice periodicity of $16.6 \pm 1.5 \text{ nm}$. Unless otherwise noted, all uncertainties and error bars represent ± 1 standard deviation.

Although each nanowire has a very high aspect ratio (length/width), the aspect ratio of each individual segment is low. In isolation, the shape anisotropy of such a flat structure favors magnetization orientation in the plane of the “pancake”. The collective behavior of the segments in an array is expected to be much more complex and has consequently been characterized using vibrating sample magnetometry (VSM). Using vector coils, we measured the magnetization perpendicular and parallel to an applied field swept between $\pm 1 \text{ T}$ (Figure 1d,e). A linear response of the magnetization above a given applied field is often associated with magnetic saturation with a paramagnetic contribution from the system (e.g., the sample holder). However, the alumina matrix is diamagnetic and the nanowire arrays may have large demagnetizing dipolar interactions. Both effects contribute to the negative slope of the magnetization at high fields in Figure 1d. Since a fully reversible alignment of the nanowire magnetization extending to extremely high fields may result in a linear response, the saturation field for the nanowires is unknown and cannot be determined from these magnetization data. The sample does not appear to saturate at fields below 1 T, as demonstrated by a net perpendicular magnetization up to 1 T in both geometries.

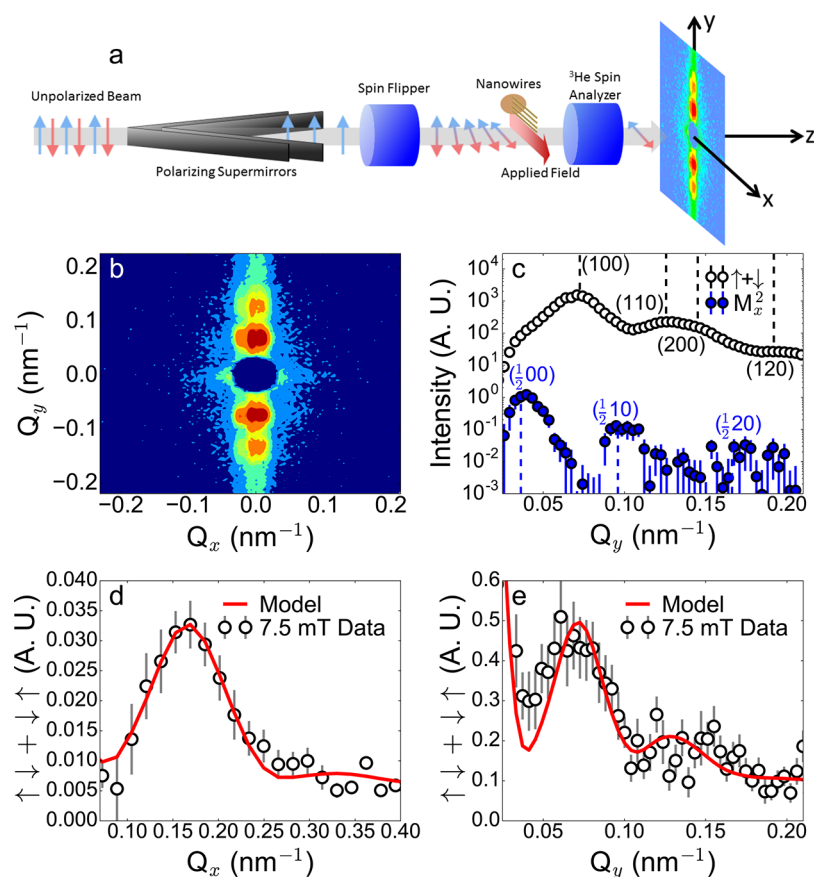


Figure 2. (a) Schematic of the beamline configuration for the PASANS measurements performed in this work. Although nanowires and applied field are shown aligned along the primary direction of interest (X), measurements were also performed with the nanowires aligned along the Y direction. (b) Typical unpolarized 2-D SANS pattern produced by this $(11.6/5.0)_{350}$ nm sample with the geometry shown in part (a). (c) Sum of the up and down intensities is proportional to $\ln(Q_y)^2$ (eq 1), shown in black. Normalized $\ln M_x(Q_y)^2$ (eq 3) is obtained from the difference (blue) of the up and down intensities for a cut through the scattering along Q_y (interwire direction) at 700 mT. Black and blue dashed lines show the theoretical peak locations for the structural and magnetic peaks, respectively. (d) Spin-flip scattering cut along the Q_x (intersegment) direction for a full-polarized measurement in the 7.5 mT field condition. (e) Spin-flip scattering cut along the Q_y (interwire) direction for a full-polarized measurement in the 7.5 mT field condition. The model fits shown in (d) and (e) are described in the [Supporting Information](#).

Having probed the bulk magnetic response by VSM, PASANS was utilized for a determination of the magnetic and structural order present in the nanowire array.^{32–35} Measurements were performed on the NG7 SANS at the NIST Center for Neutron Research, and a schematic of the typical experimental arrangement with the nanowire axis and applied magnetic field aligned along the X axis is presented in [Figure 2a](#). As described in the [Experimental Section](#), scattering trajectories along Q_y are sensitive to the interwire spacing and the corresponding magnetic correlations (as viewed perpendicular to the nanowire axis), while trajectories along Q_x are sensitive to the intersegment structural and magnetic morphology (as viewed parallel to the nanowire axis). The spin selection rules for magnetic scattering of neutrons require that magnetic scattering originates only from the component of magnetization perpendicular to the scattering vector Q .³⁶

In PASANS measurements,^{32,33} the spin state of the incident and scattered neutrons can be selected with a supermirror polarizer plus RF spin flipper and ^3He spin analyzer, respectively (see [Experimental Section](#)) allowing structural and X, Y, Z magnetic scattering to be separated. In our notation for the scattered intensity, two consecutive arrows (e.g., $\uparrow\downarrow$) indicate the up or down state of the neutron spin before and

after scattering from the sample, respectively. When both are defined, the scattering data were obtained using full-polarization (i.e., with both polarizer and analyzer). If only a single arrow is present, then the half-polarization measurement was performed with only a spin polarizer (i.e., no ^3He spin analyzer). For half-polarized scattering, $\uparrow \equiv \uparrow\uparrow + \uparrow\downarrow$ and $\downarrow \equiv \downarrow\downarrow + \downarrow\uparrow$. Half-polarization has advantages of a larger accessible Q -range and increased intensity, while full-polarization analysis can unambiguously isolate the spin-flip ($\uparrow\downarrow$ or $\downarrow\uparrow$) scattering which is entirely magnetic and can be used to directly measure the Y and Z magnetization components perpendicular to the field, B , applied parallel to the X axis.

In this geometry, the following equations for PASANS measurements with half-polarization^{32,33} show how scattered intensity can expose variations in the nuclear structure (N) and/or magnetization parallel (M_{\parallel}) and perpendicular (referred to as “in-plane”, $M_{\text{in-plane}}$) to $B \parallel$ to the nanowire (X) axis:

$$[\downarrow + \uparrow](Q_y) = \ln(Q_y)^2 + \ln M_x(Q_y)^2 + \ln M_z(Q_y)^2 \\ \approx \ln(Q_y)^2 \text{ for } N \gg M \text{ (interwire } N \text{ variations)} \quad (1)$$

$$[\downarrow - \uparrow](Q_y) = 2IN(Q_y)(M_x(Q_y)|\cos(\xi))$$

(interwire $N - M_{\parallel}$ variations) (2)

$$|M_x(Q_y)|^2 \approx (\text{eq 2})^2 / 4(\text{eq 1}) \text{ (interwire } M_{\parallel} \text{ variations)}$$

(3)

The equations for the scattered intensity from PASANS measurements with full polarization are^{32,33}

$$[\uparrow\downarrow + \downarrow\uparrow](Q_x) = |M_y(Q_x)|^2 + |M_z(Q_x)|^2$$

$= 2|M_{\text{in-plane}}(Q_x)|^2$ (intersegment $M_{\text{in-plane}}$ variations) (4)

$$[\uparrow\downarrow + \downarrow\uparrow](Q_y) = |M_z(Q_y)|^2$$

$= |M_{\text{in-plane}}(Q_y)|^2$ (interwire $M_{\text{in-plane}}$ variations) (5)

$N(Q)$ and $M(Q)$ refer to the Fourier transform of the nuclear and magnetic scattering length density (SLD) over space, respectively. X, Y, and Z subscripts of M specify the magnetization direction, while subscripts of Q specify the direction a Q -trajectory is taken through the data. The $\cos(\xi)$ term is a measure of the correlation between the $N(Q)$ and $M_x(Q)$ terms.

DISCUSSION

The most prominent features of the raw 2-D scattering shown in Figure 2b are large, clearly visible peaks along the Y axis. This band of high intensity primarily represents structural scattering corresponding to interwire spacing, as shown in Figure 2c. In the structural scattering ($|N(Q_x)|^2$) extracted using eq 1, we observe three peaks originating from the (100), (110), (200), and (120) planes of a two-dimensional hexagonal lattice with an interwire spacing of 100 nm, confirming the high-quality, short-range structural order in these nanowire arrays. To emphasize the magnetic scattering along the Q_y (interwire) direction, a difference of $\downarrow - \uparrow$ intensity divided by $|N(Q_x)|$ (eq 3) in a 700 mT field is also plotted in Figure 2c. As expected, the component of the magnetization parallel to the magnetic field ($M_x(Q_y)$) is large, while $M_z(Q_y)$ and $M_y(Q_y)$ (see Figure S9d) are negligibly small. However, the magnetic peaks in Figure 2c do not index to the structural scattering positions, but instead index to half-order positions $[(1/2, 0, 0), (1/2, 1, 0), \text{ and } (1/2, 2, 0)]$, indicating that the periodicity of M_x ($M \parallel H$) is twice that of the interwire spacing. Thus, at 700 mT the arrangement of the ordered portion of the M_x spins must either have a net moment $\parallel H$ alongside some form of antiferromagnetic interwire coupling or defects within a dominant antiferromagnetic interwire morphology such that $\cos(\varepsilon) \neq 0$ (eq 3 and Supporting Information). We expect these peaks to be replaced with peaks commensurate with $|N(Q_x)|^2$ as the applied field is increased and the wire magnetization approaches saturation. The same magnetic peaks (shown in Figure S8) are less intense at 7.5 mT and have largely disappeared closer to saturation in 1500 mT,^{37–46} indicating that the antiferromagnetic order between wires thus appears to be maximized near approximately 700 mT (Figure 2c). The absence of ferromagnetic peaks at the structural peak locations indicates that the system is not completely saturated

even at 1500 mT, consistent with the linear response of the magnetization evident in high fields (Figure 1d).

Scattering from the magnetization perpendicular to the field (M_y and M_z) is evident in the spin-flip channels at 7.5 mT, as shown in Figure 2d and e, viewed along Q_x (intersegment direction) and Q_y (interwire direction), respectively. The scattering is strong, indicating that a large fraction of the FeGa moments are aligned perpendicular to the nanowire axis. (M_y and M_z are hereafter referred to as “in-plane.”) Focusing first on the interwire in-plane magnetic structure, the spin-flip peaks in Figure 2e (eq 5) index to the structural (100) and (110) or (200) interwire spacings, consistent with ferromagnetic alignment of perpendicular components of the magnetization from one nanowire to the next. Thus, while M_x (parallel to the wire axis) interacts antiferromagnetically between wires, interwire coupling for M_y and M_z (in-plane) is ferromagnetic. Note that these spin-flip peaks (Figure 2e) appear only at low fields (Figure S9d) as expected since high fields align the magnetizations parallel to the nanowires.

Determination of the composite spin structure in low fields requires consideration of the full 2D spin-flip scattering patterns. Examining the in-plane magnetic structure along Q_x , we observe a well-defined peak in the spin-flip scattering (Figure 2d) that is present at 7.5 mT but absent at 700 mT (Figure S9). Accurate determination of this magnetic peak position relative to the superlattice periodicity is crucial for identifying the nature of the intersegment magnetic correlations. From the data in Figure 2d and related scans, the magnetic scattering peaks at 0.165 nm^{-1} , corresponding to a repeat length of $38 \pm 2 \text{ nm}$ along the nanowire axis. Half-polarization SANS measurements, shown in the Supporting Information,³⁷ suggest a superlattice periodicity of $17 \pm 5 \text{ nm}$, in excellent agreement with the periodicity extracted from TEM images ($16.6 \pm 1.5 \text{ nm}$). We therefore conclude that the magnetic periodicity corresponds to 2.1 ± 0.3 superlattice repeats. This periodicity suggests antiferromagnetic order along the wire axis of the in-plane moments in adjacent FeGa segments. In other words, there are moments that are aligned antiparallel from one FeGa/Cu pair to the next in low fields (7.5 mT).

As discussed previously, ferromagnetic interwire correlation peaks (Figure 2e) are found in the spin-flip channel centered about $Q_x = 0$ along Q_y . (Note that the sample scattering at $Q_x = 0, Q_y = 0$ is obscured by the transmitted beam and instrument beamstop.) The implicit appearance of spin-flip scattering at $Q_x = 0$ along Q_x (intersegment direction) is indicative of a net in-plane ferromagnetic moment, aligned parallel from one interwire FeGa/Cu pair to the next, that coexists with the intersegment antiferromagnetic order described above. Thus, the features in Figure 2d and e are consistent with a composite spin structure in which the in-plane moments form a fan along the nanowire axis. Specifically, these and complementary full- and half-polarization data can be described and approximately fit³² with a model where the in-plane magnetization (in the YZ plane) alternates approximately $\pm 88.7^\circ$ from one FeGa segment to the next. The best agreement with the data in Figure 2d is obtained when the magnetization components of the fan at the same depth along the wire axis are aligned ferromagnetically from one nanowire to the next. Although the obtained fan angle is very close to pure antiparallel alignment, the modeling is extremely sensitive to the deviation from pure $\pm 90^\circ$ canting, as the spin-flip structure factor and scattered

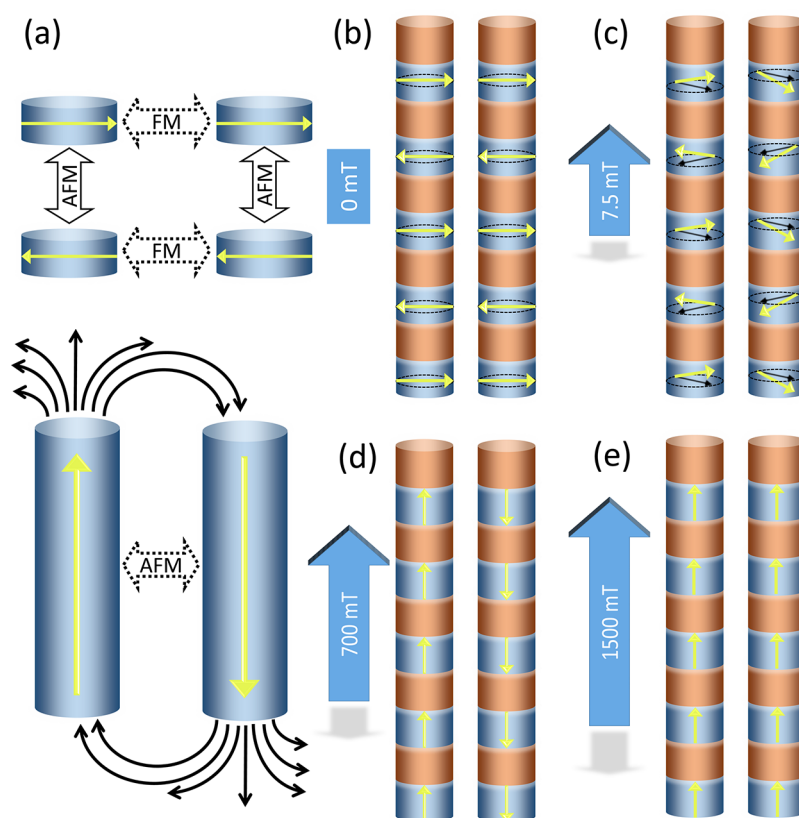


Figure 3. (a) Schematic showing the relevant ferromagnetic (FM) and antiferromagnetic (AFM) dipolar interwire (dashed) and intersegment (solid) magnetic interactions alongside schematics of the proposed magnetic structure under a (b) zero, (c) small (7.5 mT), and (d) moderate (700 mT) magnetic field applied along the nanowire axis. In (b) the magnetic moments of the FeGa segments lie in-plane (*i.e.*, perpendicular to the nanowires). In (c) they are canted to form a fan state along the nanowire axis but are ferromagnetically aligned from one wire to the next. Note that the PASANS data suggest a slight tilting of the moments out-of-plane. In (d) the components parallel to the nanowire axis are ferromagnetic between segments and antiferromagnetic among the wires. (e) Saturated magnetic state at 1500 mT for a second nanowire sample with approximate FeGa/Cu dimensions of $(46.5/19.8)_{350}$ nm.

intensity along Q_y (Figure 2e) depend directly on the deviation magnitude.

Combining the above information, proposed composite spin structures for this sample in applied fields of 0 mT, 7.5 mT, and 0.7 T are shown in Figure 3b, c, and d, respectively. Specifically, the zero-field state (not measurable with PASANS) is expected to be fully antiferromagnetic along the nanowire axis, as depicted in Figure 3b. The in-plane fan state that is stable in low fields is schematically depicted in Figure 3c. On the basis of energetic arguments and SANS data models (Supporting Information³²), we postulate that the fan state is induced by a stray in-plane field component likely from a guide field (0.15 mT) used to maintain neutron spin transport. Moderate fields (Figure 3d) rotate the magnetization toward the nanowire axis through the Zeeman interaction.

We thus propose that the ground state of the segmented nanowire array has two significant interwire interactions: antiferromagnetic alignment of the “side-by-side” magnetic units (both interwire and intersegment) and ferromagnetic alignment of the “head-to-tail” magnetic units oriented in-plane (Figure 3a). In very low fields, the ferromagnetic interwire and antiferromagnetic intrawire interactions dominate (Figure 3b and c) since the moments mostly align in the plane of the “pancake”-shaped segments. As the applied field is increased to moderate levels, the segment Zeeman energy favors moment rotation toward the nanowire axis in moderate fields. At this point antiferromagnetic interwire interactions among the

parallel moment components (Figure 3a) become significant and stabilize a magnetic structure similar to that depicted in Figure 3d. Although Figure 3d shows equal populations of nanowires with the magnetization tipped parallel and antiparallel to the applied field, the bulk magnetization and our PASANS data both indicate that a net moment along the nanowire axis also exists (*i.e.*, the number of up and down arrows are likely not equal). Upon increasing the field above 1.5 T, we expect that regions with short-range, ferromagnetically correlated nanowires reversibly coalesce into a majority domain with moments parallel to the field as shown in Figure 3e. This magnetic state is, in fact, achieved in fields of 700 and 1500 mT for a second nanowire sample with approximate FeGa/Cu dimensions of $(46.5/19.8)_{350}$ nm. Specifically, peaks in PASANS measurements of $M_x(Q_y)$, shown in Figure S11,³⁷ coincide with the structural peaks as expected for ferromagnetic order.

The sensitivity of neutrons to magnetic moments enabled the 3D domain construction in Figure 3 to be elucidated. These results are difficult to obtain by any other characterization technique, yet they are very important to the design of high-density magnetic arrays for memory and other applications.

To better understand the interplay between structure and magnetism in these nanowires, we provide a theoretical treatment of the proposed magnetic structure for the $(11.6/5.0)_{350}$ nm nanowire array.³⁷ In general, the complex magnetic properties of segmented nanowires result from the interplay

between dipolar interactions, Zeeman energy, intersegment exchange interactions, and crystalline anisotropy.⁴⁷ For FeGa nanowires, the contributions from crystalline anisotropy are insignificant. Further, RKKY exchange interactions through 5 nm of Cu are expected to be negligible due to the exponential decrease in coupling as a function of Cu thickness. Depending on segment geometry, energetics dictate that the FeGa magnetization may order in either a flower or vortex state as observed in 2-D arrays of cylinders, discs, and Ni/Cu nanowires.^{12,48–50} The vortex state is more stable in cylinders in which the magnetic segment height is a fraction of the diameter.^{12,48–50} Since the two dimensions are comparable in our system and our nanowire diameter is too small to contain a vortex core in most field orientations, we consider only the simplifying cases of magnetizations parallel and perpendicular to the wire axis in our theoretical calculations.³⁷

Consistent with investigations of related FeGa/Cu nanowire arrays,^{21,26} these calculations, detailed in the Supporting Information,³⁷ reveal that the composite magnetic structure of our nanowires follows directly from the competition between Zeeman interactions (from the field applied parallel to the wire axis) and three kinds of dipolar interactions: interwire, intrasegment, and intersegment. For nanowires with FeGa/Cu segment thicknesses of (11.6/5.0)₃₅₀ nm, these combined interactions favor in-plane magnetization in zero field and antiferromagnetic interwire coupling of field-induced moments parallel to the nanowire axis. In general, the expected behavior is similar to the magnetic order established in arrays of point dipoles, although the “pancake” segment shape gives rise to significantly weaker dipolar interactions.^{17,51} Additionally, both the ferromagnetic interwire coupling of in-plane moments and the antiferromagnetic interwire coupling of parallel moments for this sample are in agreement with theoretical expectations for planes of ferromagnetic nanocylinders.^{47,52–54} The key difference between the energetics of our segmented nanowire array and these related cylinder structures is the importance of intersegment dipolar forces that alter the easy-axis direction (Figure S2) and give rise to antiferromagnetic correlations among the in-plane magnetization components along the wire axis (Figure S3), as experimentally observed using PASANS (Figure 2d). Note that these antiferromagnetic correlations are weak, as they coexist with ferromagnetic intersegment correlations induced by a Zeeman interaction originating from a very small field component perpendicular to the wire axis.³²

These calculations support experimental observations of a gradual approach to magnetic saturation as the field is increased (Figure 1d) and highlight two magnetic configurations that can develop in the presence of an external field parallel to the nanowire axis. In high fields the segment moments are fully aligned along the nanowire axis, whereas below critical fields H_C^A and/or H_C^B the moments are tipped at a uniform angle relative to the nanowire axis. Specifically, the M_x components in all the nanowire segments are parallel and equal in the first configuration, which is stable below $H_C^A = M_0 \times 0.625$. Alternately, the second magnetic state, which is favorable below $H_C^B \approx M_0 \times 0.3$, consists of alternating rows of wires with M_x components of equal magnitude but opposite direction (Figures 3d and S5). PASANS measurements for our system show clear evidence (Figure 2c) of this second configuration persisting in a field of 0.7 T, consistent with theoretical estimates of $H_C^B \approx 0.53 T - 0.60 T$. The theoretical determination of the equilibrium configuration for this

antiparallel interwire magnetic state is complicated by the hexagonal symmetry of the alumina matrix (Figure S5). There exists significant frustration since each wire cannot simultaneously satisfy the dipolar preference for antiparallel alignment of the moments parallel to the wire axis with two closest neighboring wires. Specifically, the checkerboard alignment that occurs in square lattices is not possible in a hexagonal lattice. This frustration undoubtedly contributes to the slow approach to saturation (Figure 1d), which is associated with the antiparallel alignment of the magnetization parallel to the wire that persists to high fields (Figure S8). As in other frustrated systems such as spin ice, it is likely that a wide range of intermediate states, possibly canted (as experimentally observed) or noncollinear, are stable in the field region $0 < H < H_C^B$ as a direct consequence of the competition between the magnetic field and the dipolar interwire interaction.

CONCLUSIONS

In this work, we experimentally observed the complex intersegment and interwire magnetic interactions in high-density FeGa/Cu nanowire arrays, which are expected to serve as a basis for 3D magnetic memory and nanomechanical devices. Contrary to typical assumptions in the literature, we observe significant dipolar interwire interactions that are ferromagnetic for in-plane magnetization components and antiferromagnetic for parallel segment moments. We performed calculations of the Zeeman and dipole energies of the studied system, establishing that the interwire interactions compete with intersegment dipole interactions that are likely to be antiferromagnetic for the nanowire dimensions used here. The resulting 3D spin structure is surprisingly complex, reflecting the delicate balance among the competing energetics in the system. By incorporating additional control elements, such as wire diameter or interwire spacing, even more intricate spin structures can clearly be realized. This work not only illustrates the striking power of PASANS for *in situ* analysis of magnetic structures in nanoscale systems but also provides a model for the design and study of scalable arrays of high-density magnetic nanostructures. It thus has important ramifications for the selection of array and segment geometry in the design of next-generation spintronic, nanoelectromechanical, and nanobiomimetic devices.

EXPERIMENTAL SECTION

Nanowire Deposition. Anodized aluminum oxide templates were sputter-coated with back electrodes (20 nm Ti/200 nm Au). A rotating holder was used to expose the pore openings of each sample to the electrolyte while also connecting to the back electrode. This coated AAO was then used as a working electrode vs a Pt counter electrode in a standard three-electrode cell with a saturated calomel electrode reference. FeGa/Cu segmented nanowires were then electrodeposited using 35 mM Na₃-citrate, 15 mM FeSO₄, 17.5 mM Ga₂(SO₄)₃, and 1.5 mM CuSO₄ at room temperature and pH = 3.75 (adjusted using NaOH). The sample was rotated at 1800 rpm while the potential was alternated between -1.1 V (FeGa) and -0.8 V (Cu).

Electron Microscopy. The SEM images were taken at a 20 kV acceleration field using a JEOL 6500. The nanowires are conductive and do not require coating. For the AAO images, the back contacts (for nanowire growth) were used together with Cu tape close to the imaging to image without top coating. STEM and EDS was carried out in a JEOL ARM 200F, operated at 200 kV, equipped with an EDX octane detector (EDAX) working in line scan mode. Certain trade names and company products are identified to specify adequately the experimental procedure. In no case does such identification imply recommendation or endorsement by the National Institute of

Standards and Technology, nor does it imply that the products are necessarily the best for the purpose.

SANS. For the small-angle neutron scattering (SANS) measurements performed on NG7 at the NIST Center for Neutron Research, the nanowires were exposed to a beam of 5.5 Å wavelength (λ) neutrons with a spread of 12%. The neutrons were polarized with a double-V super mirror (efficiency of 0.998) and flipped at will using an RF flipper (efficiency of 0.993). In some of the measurements, neutrons were also spin analyzed after scattering from the sample using a polarized ^3He filter (with time-dependent efficiency between 0.997 and 0.996). The data were corrected for time-dependent polarization leakage and ^3He transmission by the process described in refs 27 and 28.^{32,33}

As shown in the instrument schematic in Figure 2a, the nanowire axes and applied magnetic fields of 0.0075, 0.7, and 1.4 T were typically aligned along the X axis (*i.e.*, perpendicular to the incident neutron beam). The scattered neutrons were collected on a position-sensitive area detector. The scattered intensity of a typical measurement was plotted as a function of transverse wave vector Q (*e.g.*, Figure 2) by taking rectangular cuts through the data along either the X or Y direction. In the small-angle limit, the wavevector Q is defined as $4\pi\theta/\lambda$ in which 2θ is the angle of the scattering on the detector relative to the incident beam direction (Z axis).

Unlike the typical samples probed with SANS, the nanowire arrays presented in this work constitute a highly oriented system along the nanowire axis but polycrystalline in the perpendicular direction. Thus, certain geometric effects must be taken into account when performing the SANS measurements and interpreting the scattering measured by the flat two-dimensional detector (Figure 2a). If a sample is rotationally invariant (*i.e.*, polycrystalline), the scattering observed at any given 2θ position on the detector is independent of the orientation of the sample relative to the incident beam. For the nanowires aligned parallel to the X axis, the interwire structure in the alumina matrix is invariant in the Y–Z plane, and $Q_y = 4\pi\theta/\lambda$ for scattering observed along the Y direction as a function of Q_y . However, the nanowire structure is not uniform in the X–Z plane. Since the incident neutron beam is fixed parallel to the Z axis, elastic scattering from the periodic intersegment order is expected at $Q_x = 4\pi\theta/\lambda$ only if the nanowires are rotated about the Y axis by θ relative to the incident beam to satisfy the Bragg scattering condition.

Thus, it is critical to ensure proper θ alignment of the nanowires along the X axis. Maintaining alignment is challenging for these low-intensity measurements, since the sample θ offset (which corresponds to the separation between Q_x and the actual scattering rod from the nanowires) increases at larger Q_x . Of course, the sensitivity of the measured intensity to a small angular offset is also highly dependent on the Q_x and Q_z resolution. Therefore, we performed measurements of the observed spin-flip peak (Figure 2d) in low fields at a series of three nanowire θ offsets across a 1° range near the ideal alignment. These measurements demonstrated that the Q_x trajectories near $\theta = 0$ fully capture the scattering along the rod parallel to the nanowire axis in the Q region relevant for this magnetic reflection. In the Q_x region of interest from 0.0 to 0.45 nm^{-1} , the introduced θ offset ranges from approximately 0.0° to 1.1° . We find that all scans show minimal shift in peak location (Figure 2d) and reach background intensity at approximately the same Q_x ($<0.45\text{ nm}^{-1}$). The invariance of the peak location with offset angle suggests that the true peak does indeed occur at very low Q , where we are highly sensitive to the scattering rod along the nanowire axis and distortions will be minimal. Thus, we find that the conclusions of this experiment are robust and not affected by either nanowire alignment.

ASSOCIATED CONTENT

Supporting Information

The Supporting Information is available free of charge on the ACS Publications website at DOI: 10.1021/acsnano.7b03488.

Supplementary figures, detailed theoretical calculations, and additional information regarding the PASANS analysis (PDF)

AUTHOR INFORMATION

Corresponding Author

*E-mail: alexander.grutter@nist.gov.

ORCID

Alexander J. Grutter: 0000-0002-6876-7625

Notes

The authors declare no competing financial interest.

ACKNOWLEDGMENTS

Access to ^3He spin filters on the NG7 30m SANS was provided by the Center for High Resolution Neutron Scattering, a partnership between the National Institute of Standards and Technology and the National Science Foundation under Agreement No. DMR-1508249. This work was supported by Office of Naval Research (ONR N00014-06-1-0530) and the National Science Foundation *via* their MRSEC (DMR-0819885) and NNIN centers, and the staff of the UMN Characterization Facility and Nanofabrication Center. The microscopy work was supported by the Research Centers in Minority Institutions Program (RCMI) Nanotechnology and Human Health Core #G12MD007591. The authors thank Jeffrey Krzywon, Dr. Shannon Watson, and Dr. Wangchun Chen for assistance with the neutron polarization and instrument operation. One of the authors (E.V.T.) is thankful to the Fulbright Foundation for financial support and to Dr. Martha Pardavi-Horvath and Dr. Robert D. McMichael for fruitful discussions.

REFERENCES

- (1) Parkin, S. S. P.; Hayashi, M.; Thomas, L. Magnetic Domain-Wall Racetrack Memory. *Science* **2008**, *320*, 190.
- (2) Allwood, D. A.; Xiong, G.; Faulkner, C. C.; Atkinson, D.; Petit, D.; Cowburn, R. P. Magnetic Domain-Wall Logic. *Science* **2005**, *309*, 1688.
- (3) Parkin, S.; Yang, S.-H. Memory on the Racetrack. *Nat. Nanotechnol.* **2015**, *10*, 195–198.
- (4) Boule, O.; Kimling, J.; Warnicke, P.; Kläui, M.; Rüdiger, U.; Malinowski, G.; Swagten, H. J. M.; Koopmans, B.; Ulysse, C.; Faini, G. Nonadiabatic Spin Transfer Torque in High Anisotropy Magnetic Nanowires with Narrow Domain Walls. *Phys. Rev. Lett.* **2008**, *101*, 216601.
- (5) Ivanov, Y. P.; Chuvilin, A.; Lopatin, S.; Kosel, J. Modulated Magnetic Nanowires for Controlling Domain Wall Motion: Toward 3D Magnetic Memories. *ACS Nano* **2016**, *10*, 5326–5332.
- (6) Rodriguez, L. A.; Bran, C.; Reyes, D.; Berganza, E.; Vázquez, M.; Gatel, C.; Snoeck, E.; Asenjo, A. Quantitative Nanoscale Magnetic Study of Isolated Diameter-Modulated FeCoCu Nanowires. *ACS Nano* **2016**, *10*, 9669–9678.
- (7) Ainslie, K. M.; Sharma, G.; Dyer, M. A.; Grimes, C. A.; Pishko, M. V. Attenuation of Protein Adsorption on Static and Oscillating Magnetostrictive Nanowires. *Nano Lett.* **2005**, *5*, 1852–1856.
- (8) Brintlinger, T.; Lim, S.-H.; Baloch, K. H.; Alexander, P.; Qi, Y.; Barry, J.; Melngailis, J.; Salamanca-Riba, L.; Takeuchi, I.; Cumings, J. *In Situ* Observation of Reversible Nanomagnetic Switching Induced by Electric Fields. *Nano Lett.* **2010**, *10*, 1219–1223.
- (9) Evans, B. A.; Shields, A. R.; Carroll, R. L.; Washburn, S.; Falvo, M. R.; Superfine, R. Magnetically Actuated Nanorod Arrays as Biomimetic Cilia. *Nano Lett.* **2007**, *7*, 1428–1434.
- (10) McGary, P. D.; Tan, L.; Zou, J.; Stadler, B. J. H.; Downey, P. R.; Flatau, A. B. Magnetic Nanowires for Acoustic Sensors (invited). *J. Appl. Phys.* **2006**, *99*, 08B310.
- (11) Reich, D. H.; Tanase, M.; Hultgren, A.; Bauer, L. A.; Chen, C. S.; Meyer, G. J. Biological Applications of Multifunctional Magnetic Nanowires (invited). *J. Appl. Phys.* **2003**, *93*, 7275–7280.

- (12) Scholz, W.; Guslienko, K. Y.; Novosad, V.; Suess, D.; Schrefl, T.; Chantrell, R. W.; Fidler, J. Transition from Single-Domain to Vortex State in Soft Magnetic Cylindrical Nanodots. *J. Magn. Magn. Mater.* **2003**, *266*, 155–163.
- (13) Zhou, Z.-g.; Liu, Z.-w. Biomimetic Cilia Based on MEMS Technology. *J. Bionic. Eng.* **2008**, *5*, 358–365.
- (14) Park, B. C.; Kim, Y. K. Synthesis, Microstructure, and Physical Properties of Metallic Barcode Nanowires. *Met. Mater. Int.* **2017**, *23*, 413–425.
- (15) Clark, A. E.; Restorff, J. B.; Wun-Fogle, M.; Lograsso, T. A.; Schlögl, D. L. Magnetostrictive Properties of Body-Centered Cubic Fe-Ga and Fe-Ga-Al Alloys. *IEEE Trans. Magn.* **2000**, *36*, 3238–3240.
- (16) Clark, A. E.; Wun-Fogle, M.; Restorff, J. B.; Lograsso, T. A.; Cullen, J. R. Effect of Quenching on the Magnetostriction on Fe 1-x Ga x (0.13 < x < 0.21). *IEEE Trans. Magn.* **2001**, *37*, 2678–2680.
- (17) Luttinger, J. M.; Tisza, L. Theory of Dipole Interaction in Crystals. *Phys. Rev.* **1946**, *70*, 954–964.
- (18) Fitzsimmons, M. R.; Bader, S. D.; Borchers, J. A.; Felcher, G. P.; Furdyna, J. K.; Hoffmann, A.; Kortright, J. B.; Schuller, I. K.; Schulthess, T. C.; Sinha, S. K.; Toney, M. F.; Weller, D.; Wolf, S. Neutron Scattering Studies of Nanomagnetism and Artificially Structured Materials. *J. Magn. Magn. Mater.* **2004**, *271*, 103–146.
- (19) Maqableh, M. M.; Huang, X.; Sung, S.-Y.; Reddy, K. S. M.; Norby, G.; Victora, R. H.; Stadler, B. J. H. Low-Resistivity 10 nm Diameter Magnetic Sensors. *Nano Lett.* **2012**, *12*, 4102–4109.
- (20) Reddy, S. M.; Park, J. J.; Na, S. M.; Maqableh, M. M.; Flatau, A. B.; Stadler, B. J. Electrochemical Synthesis of Magnetostrictive Fe-Ga/Cu Multilayered Nanowire Arrays with Tailored Magnetic Response. *Adv. Funct. Mater.* **2011**, *21*, 4677–4683.
- (21) Madhukar Reddy, S.; Jin Park, J.; Maqableh, M. M.; Flatau, A. B.; Stadler, B. J. H. Magnetization Reversal Mechanisms in 35-nm Diameter Fe1-xGax/Cu Multilayered Nanowires. *J. Appl. Phys.* **2012**, *111*, 07A920.
- (22) McGary, P. D.; Stadler, B. J. H. Electrochemical Deposition of Fe1-xGax Nanowire Arrays. *J. Appl. Phys.* **2005**, *97*, 10R503.
- (23) Encinas-Oropesa, A.; Demand, M.; Piraux, L.; Huynen, I.; Ebels, U. Dipolar Interactions in Arrays of Nickel Nanowires Studied by Ferromagnetic Resonance. *Phys. Rev. B: Condens. Matter Mater. Phys.* **2001**, *63*, 104415.
- (24) Agramunt-Puig, S.; Del-Valle, N.; Pellicer, E.; Zhang, J.; Nogués, J.; Navau, C.; Sanchez, A.; Sort, J. Modeling the Collective Magnetic Behavior of Highly-Packed Arrays of Multi-Segmented Nanowires. *New J. Phys.* **2016**, *18*, 013026.
- (25) Park, J. J.; Reddy, M.; Mudivarthi, C.; Downey, P. R.; Stadler, B. J. H.; Flatau, A. B. Characterization of the Magnetic Properties of Multilayer Magnetostrictive Iron-Gallium Nanowires. *J. Appl. Phys.* **2010**, *107*, 09A954.
- (26) Jin Park, J.; Reddy, M.; Stadler, B. J. H.; Flatau, A. B. Hysteresis Measurement of Individual Multilayered Fe-Ga/Cu Nanowires Using Magnetic Force Microscopy. *J. Appl. Phys.* **2013**, *113*, 17A331.
- (27) Jin Park, J.; Estrine, E. C.; Madhukar Reddy, S.; Stadler, B. J. H.; Flatau, A. B. Technique for Measurement of Magnetostriction in an Individual Nanowire using Atomic Force Microscopy. *J. Appl. Phys.* **2014**, *115*, 17A919.
- (28) Napolskii, K.; Eliseev, A.; Yesin, N.; Lukashin, A.; Tretyakov, Y. D.; Grigorieva, N.; Grigoriev, S.; Eckerlebe, H. Ordered Arrays of Ni Magnetic Nanowires: Synthesis and Investigation. *Phys. E (Amsterdam, Neth.)* **2007**, *37*, 178–183.
- (29) Günther, A.; Bick, J.-P.; Szary, P.; Honecker, D.; Dewhurst, C. D.; Keiderling, U.; Feoktystov, A. V.; Tschöpe, A.; Birringer, R.; Michels, A. Magnetic Field Dependent Small-Angle Neutron Scattering on a Co Nanorod Array: Evidence for Intraparticle Spin Misalignment. *J. Appl. Crystallogr.* **2014**, *47*, 992–998.
- (30) Maurer, T.; Gautrot, S.; Ott, F.; Chaboussant, G.; Zighem, F.; Cagnon, L.; Fruchart, O. Ordered Arrays of Magnetic Nanowires Investigated by Polarized Small-Angle Neutron Scattering. *Phys. Rev. B: Condens. Matter Mater. Phys.* **2014**, *89*, 184423.
- (31) Tan, L.; Stadler, B. J. H. Fabrication and Magnetic Behavior of Co/Cu Multilayered Nanowires. *J. Mater. Res.* **2006**, *21*, 2870–2875.
- (32) Krycka, K.; Chen, W.; Borchers, J.; Maranville, B.; Watson, S. Polarization-Analyzed Small-Angle Neutron Scattering. I. Polarized Data Reduction Using Pol-Corr. *J. Appl. Crystallogr.* **2012**, *45*, 546–553.
- (33) Krycka, K.; Borchers, J.; Ijiri, Y.; Booth, R.; Majetich, S. Polarization-Analyzed Small-Angle Neutron Scattering. II. Mathematical Angular Analysis. *J. Appl. Crystallogr.* **2012**, *45*, 554–565.
- (34) Krycka, K. L.; Booth, R.; Borchers, J. A.; Chen, W. C.; Conlon, C.; Gentile, T. R.; Hogg, C.; Ijiri, Y.; Laver, M.; Maranville, B. B.; Majetich, S. A.; Rhyne, J. J.; Watson, S. M. Resolving 3D Magnetism in Nanoparticles using Polarization Analyzed SANS. *Phys. B* **2009**, *404*, 2561–2564.
- (35) Krycka, K. L.; Booth, R. A.; Hogg, C. R.; Ijiri, Y.; Borchers, J. A.; Chen, W. C.; Watson, S. M.; Laver, M.; Gentile, T. R.; Dedon, L. R.; Harris, S.; Rhyne, J. J.; Majetich, S. A. Core-Shell Magnetic Morphology of Structurally Uniform Magnetite Nanoparticles. *Phys. Rev. Lett.* **2010**, *104*, 207203.
- (36) Moon, R. M.; Riste, T.; Koehler, W. C. Polarization Analysis of Thermal-Neutron Scattering. *Phys. Rev.* **1969**, *181*, 920–931.
- (37) See [Supporting Information](#), which contains refs 38–46, for additional details on the theoretical calculations and analysis of SANS data.
- (38) Fraerman, A. A.; Sapozhnikov, M. V. Metastable and Nonuniform States in 2D Orthorhombic Dipole System. *J. Magn. Magn. Mater.* **1999**, *192*, 191–200.
- (39) Guslienko, K. Y.; Choe, S.-B.; Shin, S.-C. Reorientational Magnetic Transition in High-Density Arrays of Single-Domain Dots. *Appl. Phys. Lett.* **2000**, *76*, 3609–3611.
- (40) Kline, S. Reduction and Analysis of SANS and USANS Data Using IGOR Pro. *J. Appl. Crystallogr.* **2006**, *39*, 895–900.
- (41) Mildner, D. F. R.; Barker, J. G.; Kline, S. R. The Effect of Gravity on the Resolution of Small-Angle Neutron Diffraction Peaks. *J. Appl. Crystallogr.* **2011**, *44*, 1127–1129.
- (42) Politi, P.; Pini, M. G. Dipolar Interaction Between Two-Dimensional Magnetic Particles. *Phys. Rev. B: Condens. Matter Mater. Phys.* **2002**, *66*, 214414.
- (43) Ramirez, A. Geometrically. *MRS Bull.* **2005**, *30*, 447.
- (44) Rice, S. A. Small Angle Scattering of X-rays; Guinier, A.; Fournet, G., Eds.; Translated by C. B. Wilson and with a Bibliographical Appendix by K. L. Yudowitch. Wiley: New York, 1955 268 pp. \$7.50J. *Polym. Sci.* **1956**, *19*, 594–59410.1002/pol.1956.120199326.
- (45) Schlöör, H.; Haehnel, V.; Khatri, M. S.; Srivastav, A.; Kumar, A.; Schultz, L.; Fähler, S. Magnetic Nanowires by Electrodeposition within Templates. *Phys. Status Solidi B* **2010**, *247*, 2364–2379.
- (46) Usov, N. A. Magnetization Curling in Soft Type Ferromagnetic Particles with Large Aspect Ratios. *J. Magn. Magn. Mater.* **1999**, *203*, 277–279.
- (47) Leighton, B.; Suarez, O. J.; Landeros, P.; Escrig, J. Magnetic Phase Diagrams of Barcode-Type Nanostructures. *Nanotechnology* **2009**, *20*, 385703.
- (48) Ross, C. A.; Hwang, M.; Shima, M.; Cheng, J. Y.; Farhoud, M.; Savas, T. A.; Smith, H. I.; Schwarzacher, W.; Ross, F. M.; Redjda, M.; Humphrey, F. B. Micromagnetic Behavior of Electrodeposited Cylinder Arrays. *Phys. Rev. B: Condens. Matter Mater. Phys.* **2002**, *65*, 144417.
- (49) Guo; Zhu, C.-F.; Yang, D.-L.; Chen, D.-M.; Bai, C.-L.; Wan, L.-J. Ordered Ni-Cu Nanowire Array with Enhanced Coercivity. *Chem. Mater.* **2003**, *15*, 664–667.
- (50) Chung, S. H.; McMichael, R. D.; Pierce, D. T.; Unguris, J. Phase Diagram of Magnetic Nanodisks Measured by Scanning Electron Microscopy with Polarization Analysis. *Phys. Rev. B: Condens. Matter Mater. Phys.* **2010**, *81*, 024410.
- (51) Bishop, J. E. L.; Galkin, A. Y.; Ivanov, B. A. Ground States of an Array of Magnetic Dots with Ising-Type Anisotropy and Subject to a Normal Magnetic Field. *Phys. Rev. B: Condens. Matter Mater. Phys.* **2002**, *65*, 174403.

(52) Tartakovskaya, E.; Kreuzpaintner, W.; Schreyer, A. Spin Wave Dynamics in Two- and Three-Dimensional Superlattices of Nanosized Ferromagnetic Spheres. *J. Appl. Phys.* **2008**, *103*, 023913.

(53) Tartakovskaya, E. V.; Pardavi-Horvath, M.; Vázquez, M. Configurational Spin Reorientation Phase Transition in Magnetic Nanowire Arrays. *J. Magn. Magn. Mater.* **2010**, *322*, 743–747.

(54) De La Torre Medina, J.; Darques, M.; Blon, T.; Piraux, L.; Encinas, A. Effects of Layering on the Magnetostatic Interactions in Microstructures of $\text{Co}_x\text{Cu}_{1-x}$ Nanowires. *Phys. Rev. B: Condens. Matter Mater. Phys.* **2008**, *77*, 014417.